Communications on Applied Mathematics and Computation (2022) 4:353–379
https://doi.org/10.1007/s42967-020-00118-x

ORIGINAL PAPER

Maximum-Principle-Preserving Local Discontinuous Galerkin Methods for Allen-Cahn Equations

Jie Du[1,2] · Eric Chung[3] · Yang Yang[4]

Received: 4 July 2020 / Revised: 24 November 2020 / Accepted: 26 December 2020 /
Published online: 22 April 2021

Abstract
In this paper, we study the classical Allen-Cahn equations and investigate the maximum-principle-preserving (MPP) techniques. The Allen-Cahn equation has been widely used in mathematical models for problems in materials science and fluid dynamics. It enjoys the energy stability and the maximum-principle. Moreover, it is well known that the Allen-Cahn equation may yield thin interface layer, and nonuniform meshes might be useful in the numerical solutions. Therefore, we apply the local discontinuous Galerkin (LDG) method due to its flexibility on *h-p* adaptivity and complex geometry. However, the MPP LDG methods require slope limiters, then the energy stability may not be easy to obtain. In this paper, we only discuss the MPP technique and use numerical experiments to demonstrate the energy decay property. Moreover, due to the stiff source given in the equation, we use the conservative modified exponential Runge-Kutta methods and thus can use relatively large time step sizes. Thanks to the conservative time integration, the bounds of the unknown function will not decay. Numerical experiments will be given to demonstrate the good performance of the MPP LDG scheme.

Keywords Maximum-principle-preserving · Local discontinuous Galerkin methods · Allen-Cahn equation · Conservative exponential integrations

Mathematics Subject Classification 65M12 · 65M60

✉ Yang Yang
yyang7@mtu.edu

Jie Du
jdu@tsinghua.edu.cn

Eric Chung
tschung@math.cuhk.edu.hk

[1] Yau Mathematical Sciences Center, Tsinghua University, Beijing 100084, China

[2] Yanqi Lake Beijing Institute of Mathematical Sciences and Applications, Beijing 101408, China

[3] Department of Mathematics, The Chinese University of Hong Kong, Hong Kong SAR, China

[4] Department of Mathematical Sciences, Michigan Technological University, Houghton, MI 49931, USA

1 Introduction

Gradient flows are widely used in mathematical models for problems in materials science and fluid dynamics [3, 4]. A gradient flow is usually determined by an energy functional, and a typical choice of this functional is given by

$$E(u) := \int_\Omega \Big(\frac{1}{2}|\nabla u|^2 + F(u)\Big)\mathrm{d}\mathbf{x},$$

where $\Omega \in \mathbb{R}^d\,(d = 1, 2, 3)$ is a bounded domain. For example, in the simulation of two phase dynamics, the unknown variable u represents the concentration of one of the two phases, and $F(u)$ is the nonlinear free energy density. A common choice for the function $F(u)$ is given by $\frac{1}{4\epsilon^2}(u^2 - 1)^2$ with ϵ being the inter-facial width.

In this paper, we consider the Allen-Cahn equation which can be interpreted as an L^2 gradient flow:

$$\begin{aligned} u_t &= -M\nu, \\ \nu &= \frac{\delta E}{\delta u} = -\Delta u + F'(u), \end{aligned}$$

where $M > 0$ is the mobility constant and ν is the chemical potential. For simplicity of the notations, we denote $s(u) = -MF'(u)$, then the governing equation can be rewritten into the following general form:

$$u_t = M\Delta u + s(u), \tag{1}$$

subject to the initial condition

$$u(\mathbf{x}, 0) = u_0(\mathbf{x}), \quad \mathbf{x} \in \Omega, \tag{2}$$

and periodic or homogeneous Neumann/Dirichlet boundary conditions. Here we assume $s(1) = s(-1) = 0$. Roughly speaking, the Allen-Cahn equation describes regions with $u \approx 1$ and $u \approx -1$ that grow and decay at the expense of one another.

One important property of the Allen-Cahn equation is that the energy function is decreasing with time:

$$\frac{\mathrm{d}}{\mathrm{d}t}E(u) \leqslant 0. \tag{3}$$

It is important for numerical schemes to preserve this property. The energy stability for the approximation of Allen-Cahn equations has been investigated intensively. Some popular numerical schemes are convex splitting schemes [36], stabilized schemes [33, 39], invariant energy quadratization methods [41, 42], scalar auxiliary variable (SAV) approach [31, 32], etc.

Besides, the exact solutions of the classical Allen-Cahn equations enjoy the maximum-principle, i.e., the exact solutions are between -1 and 1 if the initial condition satisfies the same property. Most of the previous works focus on the energy stability, and to the best knowledge, the only works in this direction are given in [19, 23, 30, 35], where finite difference methods were discussed. Moreover, the gradient flows may yield a thin transition layer. Therefore, nonuniform meshes are generally useful in capturing these layers. Because of these considerations, we would like to apply the discontinuous Galerkin (DG) method due to its good stability, high-order accuracy, and flexibility on h-p adaptivity and

complex geometry. Moreover, in order to preserve the maximum-principle, some slope limiters have to be applied, and the energy stability would be rather difficult to prove. In this paper, we will mainly focus on the maximum-principle-preserving (MPP) techniques and use numerical experiments to demonstrate the energy decay property.

DG methods were first introduced in [28] in the framework of neutron transportation. Subsequently, the Runge-Kutta (RK) discontinuous Galerkin (RKDG) methods for hyperbolic conservation laws were introduced in a series of papers [9–12]. For convection diffusion equations, the local discontinuous Galerkin (LDG) method was given in [13] motivated by [2], where the Navier-Stokes equations were successfully solved. Besides the above, the ultra-weak DG (UDG) method [6], the staggered DG (SDG) method [8, 14], the direct DG (DDG) method [26], the interior penalty DG (IPDG) methods [1, 29, 37] and the LDG methods on overlapping meshes [18] are also important candidates for solving convection-diffusion equations.

Recently, in [43], genuinely MPP high-order DG methods for scalar conservation laws have been constructed. For parabolic equations, the second-order MPP DG methods were given in [44]. The technique works for IPDG, LDG and UDG methods, see [22, 25] for some applications. However, the extension to high-order schemes seems to be not straightforward. The third-order MPP schemes based on LDG methods on overlapping meshes [16] and DDG method [5] were discussed. Other high-order methods were also investigated in [7, 21, 34, 38, 40] based on the modification of numerical fluxes.

It is well known that the Allen-Cahn equation contains stiff source, leading to extremely small time step size if the time integration is not constructed suitably. Recently, Huang and Shu introduced the modified exponential RK method for hyperbolic equations with stiff source terms [24]. The scheme is weakly asymptotic preserving and overcomes the stiffness. They made some assumptions on the stiff source term in order to design the bound-preserving technique. However, Allen-Cahn equations do not satisfy those assumptions. Moreover, their scheme is not conservative, i.e., if the numerical approximation at the time level n is 1, then it may not be 1 at the time level $n+1$, hence it is not suitable for Allen-Cahn equations. Later, in [15], two of the authors in this paper introduced the conservative modified exponential RK method and the third-order extension was also given in [17]. Thanks to the conservative time integrations, we can construct the MPP technique for Allen-Cahn equations. Also, the bounds of the numerical approximations will not decay by the time integrations. We will explain this conservative issue in details at the end of Sect. 2.

For simplicity of presentation, we only consider the one- and two-dimensional problems ($d = 1, 2$) in this paper. Yet our method can be extended to problems in three space dimensions ($d = 3$). Moreover, we only discuss the detailed formulation for second-order LDG schemes coupled with the second-order conservative modified exponential RK method [15] for Allan-Cahn equations. We will theoretically prove the MPP technique for our method and show that the bounds will not decay. The third-order time integration has been given in [17], and high-order spatial discretizations can be obtained following the techniques introduced in [16, 21, 34, 38]. Both second-order and third-order methods will be tested in numerical examples, which demonstrate that the time step size can be larger than the one in the traditional RK method. Moreover, we can observe the energy decays numerically.

The rest of the paper is organized as follows: we will demonstrate the LDG scheme and the time integration for the Allen-Cahn equation in one space dimension in Sect. 2. The MPP property will be proved in Sect. 3. We will extend the idea to problems in two space dimensions in Sect. 4. Numerical experiments will be given in Sect. 5. We will end in Sect. 6 with some concluding remarks.

2 Numerical Scheme in One Space Dimension

In this section, we consider the following one-dimensional Allen-Cahn equation:

$$u_t = Mu_{xx} + s(u). \tag{4}$$

We will review the LDG method for spatial derivative in Sect. 2.1. Then, we adopt the second-order conservative modified exponential RK method in Sect. 2.2 to obtain the fully discretized scheme.

2.1 LDG Spacial Discretization

We first introduce an auxiliary variable p to represent u_x and rewrite (4) into the following system of first-order equations:

$$\begin{cases} u_t = Mp_x + s(u), \\ p = u_x. \end{cases} \tag{5}$$

In order to solve the problem numerically, we decompose the computational domain Ω into non-overlapping regular cells and denote the ith cell as

$$I_i = \left[x_{i-\frac{1}{2}}, x_{i+\frac{1}{2}}\right], \quad i = 1, \cdots, N.$$

The cell center of I_i is denoted as

$$x_i = \frac{1}{2}\left(x_{i-\frac{1}{2}} + x_{i+\frac{1}{2}}\right).$$

For simplicity, we consider uniform meshes. However, this assumption is not essential. We denote the cell length as Δx:

$$\Delta x = x_{i+\frac{1}{2}} - x_{i-\frac{1}{2}}.$$

The finite element space consists of piecewise polynomials which can be discontinuous across cell boundaries:

$$V_h := \{u_h : u_h|_{I_i} \in P^k(I_i),\ i = 1, \cdots, N\},$$

where $P^k(I_i)$ is the set of all polynomials of degree up to k defined on the cell I_i. In this paper, we take $k = 1$ and consider the second-order scheme.

We multiply each equation in (5) with test functions in V_h and integrate the equation on each cell I_i. By using integration by parts, the LDG method is defined as follows: to find $u_h(\cdot, t) \in V_h$ and $p_h \in V_h$, such that for any test functions $z, q \in V_h$ and any cell I_i, we have

$$\int_{I_i} (u_h)_t z \mathrm{d}x = M\left(-\int_{I_i} p_h z_x \mathrm{d}x + \hat{p}_{i+\frac{1}{2}} z^-_{i+\frac{1}{2}} - \hat{p}_{i-\frac{1}{2}} z^+_{i-\frac{1}{2}}\right) + \int_{I_i} s(u_h) z \mathrm{d}x, \tag{6}$$

$$\int_{I_i} p_h q \mathrm{d}x = -\int_{I_i} u_h q_x \mathrm{d}x + \hat{u}_{i+\frac{1}{2}} q^-_{i+\frac{1}{2}} - \hat{u}_{i-\frac{1}{2}} q^+_{i-\frac{1}{2}}, \tag{7}$$

where the notations $w^-_{i+\frac{1}{2}}$ and $w^+_{i+\frac{1}{2}}$ are used to represent the values of a function w on the point $x_{i+\frac{1}{2}}$ obtained from the left and the right of $x_{i+\frac{1}{2}}$, respectively. $\hat{p}_{i+\frac{1}{2}}$ and $\hat{u}_{i+\frac{1}{2}}$ are the numerical fluxes and are taken as alternating fluxes

$$\hat{u}_{i+\frac{1}{2}} = u^-_{i+\frac{1}{2}}, \quad \hat{p}_{i+\frac{1}{2}} = p^+_{i+\frac{1}{2}}, \tag{8}$$

or

$$\hat{u}_{i+\frac{1}{2}} = u^+_{i+\frac{1}{2}}, \quad \hat{p}_{i+\frac{1}{2}} = p^-_{i+\frac{1}{2}}. \tag{9}$$

In the remaining part of this paper, we adopt (8). The proof for (9) is similar.

2.2 Conservative Modified Exponential RK Temporal Discretization

It is easy to solve for p_h locally on each cell I_i by using (7) to get

$$p_h(x)|_{I_i} = \frac{u^-_{i+\frac{1}{2}} - u^-_{i-\frac{1}{2}}}{\Delta x} + \frac{6(x-x_i)}{\Delta x^2}\left(u^-_{i-\frac{1}{2}} - u^+_{i-\frac{1}{2}}\right),$$

and hence we have

$$\hat{p}_{i-\frac{1}{2}} = p^+_{i-\frac{1}{2}} = \frac{u^-_{i+\frac{1}{2}} + 3u^+_{i-\frac{1}{2}} - 4u^-_{i-\frac{1}{2}}}{\Delta x}.$$

Substituting the above equations into (6) and noticing that

$$z_x|_{I_i} = \frac{z^-_{i+\frac{1}{2}} - z^+_{i-\frac{1}{2}}}{\Delta x}$$

is a constant, we get the following semi-discrete scheme for solving $u_h(x,t)$ on I_i:

$$\begin{aligned}\frac{\mathrm{d}}{\mathrm{d}t}\int_{I_i} u_h(x,t)z(x)\mathrm{d}x = \frac{M}{\Delta x}\left[\left(u^-_{i+\frac{3}{2}} + 3u^+_{i+\frac{1}{2}} - 5u^-_{i+\frac{1}{2}} + u^-_{i-\frac{1}{2}}\right)z^-_{i+\frac{1}{2}} - 3\left(u^+_{i-\frac{1}{2}} - u^-_{i-\frac{1}{2}}\right)z^+_{i-\frac{1}{2}}\right] \\ + \int_{I_i} s(u_h)z(x)\mathrm{d}x, \quad \forall z(x) \in V_h,\ i = 1, \cdots, N.\end{aligned}$$

For simplicity of the formulation, we introduce the notation

$$F_i(u_h, z) = \frac{M}{\Delta x}\left[\left(u^-_{i+\frac{3}{2}} + 3u^+_{i+\frac{1}{2}} - 5u^-_{i+\frac{1}{2}} + u^-_{i-\frac{1}{2}}\right)z^-_{i+\frac{1}{2}} - 3\left(u^+_{i-\frac{1}{2}} - u^-_{i-\frac{1}{2}}\right)z^+_{i-\frac{1}{2}}\right],$$

and use $(\cdot,\cdot)_{I_i}$ to denote the inner product on $L^2(I_i)$. Then, the semi-discrete scheme becomes

$$\frac{\mathrm{d}}{\mathrm{d}t}\left(u_h, z\right)_{I_i} = F_i(u_h, z) + \left(s(u_h), z\right)_{I_i}, \quad \forall z(x) \in V_h,\ i = 1, \cdots, N. \tag{10}$$

Since the source term can be stiff, we apply the second-order conservative modified exponential RK method [15] (without the expansion of exponential terms) to get the fully discretized scheme:

$$\left(u_h^{(1)}, z\right)_{I_i} = B_1^1\left[\left(u_h^n, z\right)_{I_i} + \Delta t F_i(u_h^n, z) + \Delta t\left(s(u_h^n) + \mu u_h^n, z\right)_{I_i}\right], \tag{11}$$

$$\left(u_h^{n+1}, z\right)_{I_i} = B_2^1\left(u_h^n, z\right)_{I_i} + B_2^2\left[\left(u_h^{(1)}, z\right)_{I_i} + \Delta t F_i(u_h^{(1)}, z) + \Delta t\left(s(u_h^{(1)}) + \mu u_h^{(1)}, z\right)_{I_i}\right], \tag{12}$$

where $u_h^n(x)$ is the numerical approximation of $u_h(x,t)$ at the time level n, and $u_h^{(1)}(x)$ is a middle stage approximation. Here μ is a constant to be determined in each time step and may depend on the time level n, and

$$B_1^1 = \frac{1}{1+\mu\Delta t}, \quad B_2^1 = \frac{\mathrm{e}^{-\mu\Delta t}}{\mathrm{e}^{-\mu\Delta t}+1+\mu\Delta t}, \quad B_2^2 = \frac{1}{\mathrm{e}^{-\mu\Delta t}+1+\mu\Delta t}.$$

Numerical examples in Sect. 5 will show that the time step size of this method can be larger than the one used in the traditional RK methods.

We illustrate the conservative property of our method in the following theorem.

Theorem 1 *The fully discretized scheme* (11) *and* (12) *for solving Allen-Cahn equations is conservative in the sense that*: *if the numerical solution* u_h^n *reaches the upper bound* 1 (*or the lower bound* -1) *at the time level* n, *then* $u_h^{n+1}(x)$ *remains* 1 (*or* -1) *at the time level* $n+1$.

Proof It is easy to check the following important property for our method:

$$(1+\mu\Delta t)B_1^1 = 1, \quad B_2^1 + (1+\mu\Delta t)B_2^2 = 1. \tag{13}$$

By the definition of F_i, we know that $F_i(u_h, z) = 0$ for a constant function u_h. Also, we have assumed that $s(1) = s(-1) = 0$ for the Allen-Cahn equation. Hence, when $u_h^n = 1$ (or -1), we have $F_i(u_h^n, z) = s(u_h^n) = 0$. Then, the property (13) guarantees that

$$u_h^{(1)}(x) = u_h^n(x).$$

Subsequently, $u_h^{(1)}(x) = 1$ (or -1) will lead to $F_i(u_h^{(1)}, z) = s(u_h^{(1)}) = 0$, and (12) together with the property (13) gives

$$u_h^{n+1}(x) = u_h^{(1)}(x) = u_h^n(x).$$

Hence, $u_h^{n+1}(x)$ remains 1 (or -1) at time level $n+1$.

Remark 1 The major difference between our temporal discretization and the modified exponential RK methods [24] is the design of the coefficients in (11) and (12). The coefficients in [24] do not satisfy the property (13) and hence the magnitudes of the solutions may decay with time due to the dissipation of the source term.

Remark 2 As we see in the next section, the conservative property (13) will also be used for designing the MPP technique. For the non-conservative method in [24], the MPP

technique is relatively more complicated and some extra conditions on the source term are needed.

The third-order time integration [17] for solving (10) is

$$\begin{aligned}
\left(u_h^{(1)},z\right)_{I_i} =& \left[\alpha_{10}\left(u_h^n,z\right)_{I_i}+\beta_{10}\Delta t F_i(u_h^n,z)+\beta_{10}\Delta t\left(s(u_h^n)+\mu u_h^n,z\right)_{I_i}\right]/A_1,\\
\left(u_h^{(2)},z\right)_{I_i} =& \left[\alpha_{20}\left(u_h^n,z\right)_{I_i}+\beta_{20}\Delta t F_i(u_h^n,z)+\beta_{20}\Delta t\left(s(u_h^n)+\mu u_h^n,z\right)_{I_i}\right]/A_2\\
&+\mathrm{e}^{\beta_{10}\mu\Delta t}\left[\alpha_{21}\left(u_h^{(1)},z\right)_{I_i}+\beta_{21}\Delta t F_i(u_h^{(1)},z)+\beta_{21}\Delta t\left(s(u_h^{(1)})+\mu u_h^{(1)},z\right)_{I_i}\right]/A_2,\\
\left(u_h^{n+1},z\right)_{I_i} =& \left[\alpha_{30}\left(u_h^n,z\right)_{I_i}+\beta_{30}\Delta t F_i(u_h^n,z)+\beta_{30}\Delta t\left(s(u_h^n)+\mu u_h^n,z\right)_{I_i}\right]/A_3\\
&+\mathrm{e}^{\beta_{10}\mu\Delta t}\left[\alpha_{31}\left(u_h^{(1)},z\right)_{I_i}+\beta_{31}\Delta t F_i(u_h^{(1)},z)+\beta_{31}\Delta t\left(s(u_h^{(1)})+\mu u_h^{(1)},z\right)_{I_i}\right]/A_3,\\
&+\mathrm{e}^{A\mu\Delta t}\left[\alpha_{32}\left(u_h^{(2)},z\right)_{I_i}+\beta_{32}\Delta t F_i(u_h^{(2)},z)+\beta_{32}\Delta t\left(s(u_h^{(2)})+\mu u_h^{(2)},z\right)_{I_i}\right]/A_3,
\end{aligned}$$

where

$$\begin{aligned}
\alpha_{10} =& 1, \quad \beta_{10} = 0.707\,193\,337\,692\,501\,4,\\
\alpha_{20} =& 0.668\,689\,293\,307\,440\,4, \quad \beta_{20} = 0,\\
\alpha_{21} =& 0.331\,310\,706\,692\,559\,6, \quad \beta_{21} = 0.417\,804\,756\,491\,506\,5,\\
\alpha_{30} =& 0.348\,741\,943\,025\,609\,0, \quad \beta_{30} = 0,\\
\alpha_{31} =& 0.203\,957\,613\,878\,089\,8, \quad \beta_{31} = 0,\\
\alpha_{32} =& 0.447\,300\,443\,096\,301\,1, \quad \beta_{32} = 0.564\,075\,463\,710\,043\,9,
\end{aligned}$$

and

$$\begin{aligned}
A_1 =& \alpha_{10}+\beta_{10}\mu\Delta t, \qquad A_2 = \alpha_{20}+\beta_{20}\mu\Delta t+\mathrm{e}^{\beta_{10}\mu\Delta t}\left(\alpha_{21}+\beta_{21}\mu\Delta t\right),\\
A_3 =& \alpha_{30}+\beta_{30}\mu\Delta t+\mathrm{e}^{\beta_{10}\mu\Delta t}\left(\alpha_{31}+\beta_{31}\mu\Delta t\right)+\mathrm{e}^{A\mu\Delta t}\left(\alpha_{32}+\beta_{32}\mu\Delta t\right).
\end{aligned}$$

One can also check that this scheme is conservative. For simplicity, we will only show the MPP technique for the second-order scheme. The idea can be easily extended to the third-order scheme.

3 Maximum-Principle-Preserving Technique

In this section, we design the MPP technique for our method. We will first show that the cell average values can be bounded between -1 and 1 under suitable conditions in Sect. 3.1. Then we adopt a slope limiter to make the entire solutions be bounded between -1 and 1 in Sect. 3.2.

3.1 Maximum-Principle-Preserving of the Cell Averages

We denote the cell integral average values of u_h and $s(u_h)$ on cell I_i as

$$\bar{u}_i(t) = \frac{1}{\Delta x}\int_{I_i} u_h(x,t)\mathrm{d}x, \quad \bar{s}_i(u_h) = \frac{1}{\Delta x}\int_{I_i} s(u_h)\mathrm{d}x.$$

Taking $z = 1$ in (11) and (12), we get the following equations for updating $\bar{u}_i$ in time:

$$\bar{u}_i^{(1)} = B_1^1\left[\bar{u}_i^n + \Delta t f(u_h^n)\right] + \Delta t B_1^1\left[\bar{s}_i(u_h^n) + \mu\bar{u}_i^n\right], \tag{14}$$

$$\bar{u}_i^{n+1} = B_2^1\bar{u}_i^n + B_2^2\left[\bar{u}_i^{(1)} + \Delta t f(u_h^{(1)})\right] + \Delta t B_2^2\left[\bar{s}_i(u_h^{(1)}) + \mu\bar{u}_i^{(1)}\right], \tag{15}$$

where $\bar{u}_i^n$ and $\bar{u}_i^{(1)}$ are the cell averages of u_h^n and $u_h^{(1)}$, respectively. Moreover,

$$f(\omega) = \frac{1}{\Delta x}F_i(\omega,1) = \frac{M}{\Delta x^2}\left(\omega^-_{i+\frac{3}{2}} + 3\omega^+_{i+\frac{1}{2}} - 5\omega^-_{i+\frac{1}{2}} - 3\omega^+_{i-\frac{1}{2}} + 4\omega^-_{i-\frac{1}{2}}\right)$$

for any function $\omega \in V_h$.

We first state the property of the spatial discretization operator f in the lemma below following [44].

Lemma 1 *For any function $\omega(x) \in V_h$ with $\omega(x) \in [-1,1]$, $\forall x \in I_i$, $i = 1,\cdots,N$, we have*

$$\bar{\omega}_i + \Delta t f(\omega) \in [-1,1]$$

under the CFL condition $M\frac{\Delta t}{\Delta x^2} \leqslant \frac{1}{10}$.

Proof Notice that ω is simply a linear function on each cell I_i, and hence we have

$$\bar{\omega}_i = \frac{1}{2}\left(\omega^-_{i+\frac{1}{2}} + \omega^+_{i-\frac{1}{2}}\right).$$

Then, we obtain

$$\bar{\omega}_i + \Delta t f(\omega) = a_1\omega^-_{i+\frac{3}{2}} + a_2\omega^+_{i+\frac{1}{2}} + a_3\omega^-_{i+\frac{1}{2}} + a_4\omega^+_{i-\frac{1}{2}} + a_5\omega^-_{i-\frac{1}{2}},$$
$$a_1 = \frac{M\Delta t}{\Delta x^2},\ a_2 = 3\frac{M\Delta t}{\Delta x^2},\ a_3 = \frac{1}{2} - 5\frac{M\Delta t}{\Delta x^2},\ a_4 = \frac{1}{2} - 3\frac{M\Delta t}{\Delta x^2},\ a_5 = 4\frac{M\Delta t}{\Delta x^2}.$$

It is easy to check that $a_1 + a_2 + a_3 + a_4 + a_5 = 1$. Under the condition $M\frac{\Delta t}{\Delta x^2} \leqslant \frac{1}{10}$, all coefficients are non-negative. Hence, we have written $\bar{\omega}_i + \Delta t f(\omega)$ as a convex combination of five point values of ω. Since all point values are bounded between -1 and 1, we can obtain the conclusion of this lemma.

Next, we are able to prove the MPP property for the cell averages. In the following, we consider the L-point Gaussian quadrature rule on the cell I_i, which is exact for the integral of polynomials of degree up to $2L-1$. We denote the set of these quadrature points on I_i as

$$S_i = \left\{x_1^i, x_2^i, \cdots, x_L^i\right\}.$$

Let c_α be the quadrature weights for the interval $[-0.5, 0.5]$ such that $\sum_{\alpha=1}^{L} c_\alpha = 1$. We choose L large enough such that $\bar{s}_i(u_h)$ can be approximated accurately. For the common choice $s(u) = \frac{M}{\epsilon^2}(u - u^3)$, we take $L = 2$ since u_h is a linear polynomial.

Theorem 2 *The numerical scheme* (14) *and* (15) *is MPP: if* $-1 \leqslant u_h^n(x) \leqslant 1$ *on each cell* I_i, $i = 1, \cdots, N$, *then we have* $-1 \leqslant \bar{u}_i^{(1)} \leqslant 1$ *under the conditions*

$$\mu \geqslant \max\left\{0, \max_{x\in S_i} \frac{s\left(u_h^n(x)\right)}{1-u_h^n(x)}, \max_{x\in S_i} \frac{s\left(u_h^n(x)\right)}{-1-u_h^n(x)}\right\} \qquad \text{and} \qquad M\frac{\Delta t}{\Delta x^2} \leqslant \frac{1}{10}.$$

In addition to the above conditions, if $-1 \leqslant u_h^{(1)}(x) \leqslant 1$ *on each cell* I_i, $i = 1, \cdots, N$, *and*

$$\mu \geqslant \max\left\{0, \max_{x\in S_i} \frac{s\left(u_h^{(1)}(x)\right)}{1-u_h^{(1)}(x)}, \max_{x\in S_i} \frac{s\left(u_h^{(1)}(x)\right)}{-1-u_h^{(1)}(x)}\right\},$$

then we have $-1 \leqslant \bar{u}_i^{n+1} \leqslant 1$.

Proof We only prove $-1 \leqslant \bar{u}_i^{(1)} \leqslant 1$, since the proof for $-1 \leqslant \bar{u}_i^{n+1} \leqslant 1$ can be obtained following the same line. From (14), we get

$$\bar{u}_i^{(1)} = B_1^1 R_1 + \mu\Delta t B_1^1 R_2,$$

where

$$R_1 = \bar{u}_i^n + \Delta t f(u_h^n), \qquad R_2 = \frac{1}{\mu}\bar{s}_i(u_h^n) + \bar{u}_i^n.$$

Next, we estimate the bounds of R_1 and R_2, respectively. Since $-1 \leqslant u_h^n(x) \leqslant 1$ and $M\frac{\Delta t}{\Delta x^2} \leqslant \frac{1}{10}$, we can get

$$R_1 = \bar{u}_i^n + \Delta t f(u_h^n) \in [-1, 1]$$

by using Lemma 1. Moreover, the condition of μ gives

$$-1 \leqslant \frac{1}{\mu} s\left(u_h^n(x_\alpha^i)\right) + u_h^n(x_\alpha^i) \leqslant 1, \quad \alpha = 1, \cdots, L.$$

Then, by using the Gauss quadrature rule, we get

$$R_2 = \sum_{\alpha=1}^{L} c_\alpha \left[\frac{1}{\mu} s\left(u_h^n(x_\alpha^i)\right) + u_h^n(x_\alpha^i)\right] \in [-1, 1].$$

Recall that our scheme is conservative and $(1 + \mu\Delta t)B_1^1 = 1$. Also, both B_1^1 and $\mu\Delta t B_1^1$ are non-negative. Hence, $\bar{u}_i^{(1)}$ is a convex combination of R_1 and R_2. Since $R_1, R_2 \in [-1, 1]$, we get

$$-1 \leqslant \bar{u}_i^{(1)} \leqslant 1.$$

Remark 3 In addition to the assumption $s(1) = s(-1) = 0$, we also require the following two limits:

$$\lim_{u\to 1} \frac{s(u)}{1-u}, \quad \lim_{u\to -1} \frac{s(u)}{1+u}$$

exist. Therefore, the lower bounds of μ given in the above theorem are well-defined.

3.2 Maximum-Principle-Preserving Limiter

Based on the theorem in the last section, we can construct physically relevant numerical cell averages $\bar{u}_i$. However, the polynomial u_h may be out of the bounds. Hence, we need to apply suitable limiters to $u_h^{(1)}(x)$ and $u_h^{n+1}(x)$, and construct physically relevant numerical approximations in each RK stage.

Assume that we already have $-1 \leqslant u_h^n(x) \leqslant 1$ on each cell on time level n. The full algorithm on each fixed cell I_i from time level n to time level $n+1$ is given below.

(i) Compute the first stage of the conservative time integration (11) to get $u_h^{(1)}(x)$. Since $-1 \leqslant u_h^n(x) \leqslant 1$, Theorem 2 shows that $-1 \leqslant \bar{u}_i^{(1)} \leqslant 1$ under the suitable conditions on Δt and μ.

(ii) Replace the polynomial $u_h^{(1)}|_{I_i}$ by a modified polynomial $\tilde{u}_h^{(1)}(x) \in P^1(I_i)$:

$$\tilde{u}_h^{(1)}(x) = \theta\left(u_h^{(1)}(x) - \bar{u}_i^{(1)}\right) + \bar{u}_i^{(1)},$$

where

$$\theta = \min\left\{1, \frac{1-\bar{u}_i^{(1)}}{M_i - \bar{u}_i^{(1)}}, \frac{\bar{u}_i^{(1)}+1}{\bar{u}_i^{(1)} - m_i}\right\}$$

with

$$M_i = \max_{x\in I_i} u_h^{(1)}(x), \quad m_i = \min_{x\in I_i} u_h^{(1)}(x).$$

In [43], the authors proved that the new polynomial $\tilde{u}_h^{(1)}(x)$ is still a second-order accurate approximation with the same cell average and $\tilde{u}_h^{(1)}(x) \in [-1, 1]$, for all $x \in I_i$.

(iii) Compute the second stage of the conservative time integration (12) to get $u_h^{n+1}(x)$. Since we have replaced $u_h^{(1)}(x)$ with $\tilde{u}_h^{(1)}(x)$ and $-1 \leqslant \tilde{u}_h^{(1)}(x) \leqslant 1$, we can get $-1 \leqslant \bar{u}_i^{n+1} \leqslant 1$ under the suitable conditions by using Theorem 2 again.

(iv) Replace the polynomial u_h^{n+1} on I_i by a modified polynomial $\tilde{u}_h^{n+1}(x)$:

$$\tilde{u}_h^{n+1}(x) = \theta\left(u_h^{n+1}(x) - \bar{u}_i^{n+1}\right) + \bar{u}_i^{n+1},$$

where

$$\theta = \min\left\{1, \frac{1-\bar{u}_i^{n+1}}{M_i - \bar{u}_i^{n+1}}, \frac{\bar{u}_i^{n+1}+1}{\bar{u}_i^{n+1} - m_i}\right\}, \quad M_i = \max_{x\in I_i} u_h^{n+1}(x), \quad m_i = \min_{x\in I_i} u_h^{n+1}(x).$$

Then, we can get $-1 \leqslant \tilde{u}_h^{n+1}(x) \leqslant 1$.

4 Two-Dimensional Problem

In this section, we extend the technique to two-dimensional Allen-Cahn problem (1). We first give the numerical scheme in Sect. 4.1 and then design the MPP technique in Sect. 4.2.

4.1 Numerical Scheme

We first use the classical LDG method to discrete the space and get the semi-discrete scheme. For two-dimensional problem, we need to introduce two auxiliary variables p and q to represent u_x and u_y, respectively. Thus, we can rewrite (1) into the following system:

$$\begin{cases} u_t = M(p_x + q_y) + s(u), \\ p = u_x, \\ q = u_y. \end{cases} \tag{16}$$

Suppose the computational domain is $\Omega = [a, b] \times [c, d]$. We decompose it into regular rectangular cells. Let $a = x_{\frac{1}{2}} < x_{\frac{3}{2}} < \cdots < x_{N_x+\frac{1}{2}} = b$ and $c = y_{\frac{1}{2}} < y_{\frac{3}{2}} < \cdots < y_{N_y+\frac{1}{2}} = d$ be grid points in x and y directions, respectively. We denote the (i, j)th cell as

$$I_{i,j} = \left[x_{i-\frac{1}{2}}, x_{i+\frac{1}{2}}\right] \times \left[y_{j-\frac{1}{2}}, y_{j+\frac{1}{2}}\right], \quad i = 1, \cdots, N_x,\ j = 1, \cdots, N_y.$$

For simplicity, we also make a non-essential assumption of uniform mesh and denote the cell lengths in x and y directions as Δx and Δy, respectively. The finite element space consists of piecewise polynomials which can be discontinuous across cell boundaries:

$$V_h := \left\{ u_h : u_h|_{I_{i,j}} \in Q^1(I_{i,j}),\ i = 1, \cdots, N_x,\ j = 1, \cdots, N_y \right\}.$$

For any function $v \in V_h$, we denote $v^+_{i-\frac{1}{2},j}$, $v^-_{i+\frac{1}{2},j}$, $v^+_{i,j-\frac{1}{2}}$ and $v^-_{i,j+\frac{1}{2}}$ to be the traces of $v|_{I_{i,j}}$ on the four edges of $I_{i,j}$, respectively. The LDG method in two-dimensional space is defined as follows: to find $\left(u_h(\cdot, t), p_h, q_h\right) \in [V_h]^3$, such that for any test functions $(v, w, z) \in [V_h]^3$ and any cell $I_{i,j}$, we have

$$\begin{aligned} \int_{I_{i,j}} (u_h)_t v \mathrm{d}x\mathrm{d}y = &-M \int_{I_{i,j}} (p_h v_x + q_h v_y) \mathrm{d}x\mathrm{d}y + \int_{I_{i,j}} s(u_h) v \mathrm{d}x\mathrm{d}y \\ &+ M \int_{y_{j-\frac{1}{2}}}^{y_{j+\frac{1}{2}}} \left(\hat{p}_{i+\frac{1}{2},j} v^-_{i+\frac{1}{2},j} - \hat{p}_{i-\frac{1}{2},j} v^+_{i-\frac{1}{2},j} \right) \mathrm{d}y \\ &+ M \int_{x_{i-\frac{1}{2}}}^{x_{i+\frac{1}{2}}} \left(\hat{q}_{i,j+\frac{1}{2}} v^-_{i,j+\frac{1}{2}} - \hat{q}_{i,j-\frac{1}{2}} v^+_{i,j-\frac{1}{2}} \right) \mathrm{d}x, \end{aligned} \tag{17}$$

$$\int_{I_{i,j}} p_h w \mathrm{d}x\mathrm{d}y = -\int_{I_{i,j}} u_h w_x \mathrm{d}x\mathrm{d}y + \int_{y_{j-\frac{1}{2}}}^{y_{j+\frac{1}{2}}} \left(\hat{u}_{i+\frac{1}{2},j} w^-_{i+\frac{1}{2},j} - \hat{u}_{i-\frac{1}{2},j} w^+_{i-\frac{1}{2},j} \right) \mathrm{d}y, \tag{18}$$

$$\int_{I_{i,j}} q_h z \mathrm{d}x\mathrm{d}y = -\int_{I_{i,j}} u_h z_x \mathrm{d}x\mathrm{d}y + \int_{x_{i-\frac{1}{2}}}^{x_{i+\frac{1}{2}}} \left(\hat{u}_{i,j+\frac{1}{2}} z^-_{i,j+\frac{1}{2}} - \hat{u}_{i,j-\frac{1}{2}} z^+_{i,j-\frac{1}{2}} \right) \mathrm{d}x, \tag{19}$$

where the numerical fluxes are taken as alternating fluxes

$$\hat{u}_{i+\frac{1}{2},j} = u^-_{i+\frac{1}{2},j}, \quad \hat{u}_{i,j+\frac{1}{2}} = u^-_{i,j+\frac{1}{2}}, \quad \hat{p}_{i+\frac{1}{2},j} = p^+_{i+\frac{1}{2},j}, \quad \hat{q}_{i,j+\frac{1}{2}} = q^+_{i,j+\frac{1}{2}}.$$

After we get the semi-discrete scheme by using the LDG method, we still use the second-order conservative modified exponential RK method (11) and (12) to march in time.

4.2 Maximum-Principle-Preserving Technique

We first solve for p_h locally on each cell $I_{i,j}$ by using (18). For the integral on $[y_{j-\frac{1}{2}}, y_{j+\frac{1}{2}}]$, we use the two-point Gaussian quadrature. We denote the two quadrature points on $[y_{j-\frac{1}{2}}, y_{j+\frac{1}{2}}]$ as y^j_1 and y^j_2 and denote the two quadrature weights on $[-0.5, 0.5]$ as c_1 and c_2. Moreover, we denote the linear interpolation basis functions as $\phi_1(y)$ and $\phi_2(y)$, $y \in [y_{j-\frac{1}{2}}, y_{j+\frac{1}{2}}]$, such that

$$\phi_m(y^j_n) = \delta_{mn}, \quad m, n \in \{1, 2\}.$$

In (18), we take $w(x, y) = \tilde{w}(x)\phi_m(y) \in Q^1(I_{i,j})$, $m = 1, 2$, where $\tilde{w}(x)$ can be any function in $P^1([x_{i-\frac{1}{2}}, x_{i+\frac{1}{2}}])$. Then, we get

$$\begin{aligned} &\int_{x_{i-\frac{1}{2}}}^{x_{i+\frac{1}{2}}} p_h\left(x, y^j_m\right)\tilde{w}(x)\mathrm{d}x \\ &= -\int_{x_{i-\frac{1}{2}}}^{x_{i+\frac{1}{2}}} u_h\left(x, y^j_m\right)\tilde{w}_x(x)\mathrm{d}x + \hat{u}_{i+\frac{1}{2},j}\left(y^j_m\right)\tilde{w}^-_{i+\frac{1}{2}} - \hat{u}_{i-\frac{1}{2},j}\left(y^j_m\right)\tilde{w}^+_{i-\frac{1}{2}}, \quad m = 1, 2, \end{aligned}$$

for any test function $\tilde{w}(x) \in P^1([x_{i-\frac{1}{2}}, x_{i+\frac{1}{2}}])$, which is similar to the one-dimensional problem (7). Following the same idea as in the one-dimensional case, we get

$$\hat{p}_{i-\frac{1}{2},j}\left(y^j_m\right) = p^+_{i-\frac{1}{2},j}\left(y^j_m\right) = \frac{u^-_{i+\frac{1}{2},j}\left(y^j_m\right) + 3u^+_{i-\frac{1}{2},j}\left(y^j_m\right) - 4u^-_{i-\frac{1}{2},j}\left(y^j_m\right)}{\Delta x}, \quad m = 1, 2. \tag{20}$$

Similarly, we can solve for q_h locally on each cell $I_{i,j}$ by using (19) and get

$$\hat{q}_{i,j-\frac{1}{2}}\left(x^i_m\right) = q^+_{i,j-\frac{1}{2}}\left(x^i_m\right) = \frac{u^-_{i,j+\frac{1}{2}}\left(x^i_m\right) + 3u^+_{i,j-\frac{1}{2}}\left(x^i_m\right) - 4u^-_{i,j-\frac{1}{2}}\left(x^i_m\right)}{\Delta y}, \quad m = 1, 2, \tag{21}$$

where x^i_1 and x^i_2 are the two Gaussian quadrature points on $[x_{i-\frac{1}{2}}, x_{i+\frac{1}{2}}]$.

Taking $v = 1$ in (17), we get

$$\int_{I_{i,j}} (u_h)_t \mathrm{d}x\mathrm{d}y = M \int_{y_{j-\frac{1}{2}}}^{y_{j+\frac{1}{2}}} \left(\hat{p}_{i+\frac{1}{2},j} - \hat{p}_{i-\frac{1}{2},j}\right)\mathrm{d}y + M \int_{x_{i-\frac{1}{2}}}^{x_{i+\frac{1}{2}}} \left(\hat{q}_{i,j+\frac{1}{2}} - \hat{q}_{i,j-\frac{1}{2}}\right)\mathrm{d}x + \int_{I_{i,j}} s(u_h)\mathrm{d}x\mathrm{d}y.$$

By using the two-point Gaussian quadrature rule, we obtain

$$\frac{\mathrm{d}}{\mathrm{d}t}\bar{u}_{i,j} = \frac{M}{\Delta x}\sum_{m=1}^{2} c_m \left[\hat{p}_{i+\frac{1}{2},j}\left(y_m^j\right) - \hat{p}_{i-\frac{1}{2},j}\left(y_m^j\right)\right] + \frac{M}{\Delta y}\sum_{m=1}^{2} c_m \left[\hat{q}_{i,j+\frac{1}{2}}\left(x_m^i\right) - \hat{q}_{i,j-\frac{1}{2}}\left(x_m^i\right)\right] + \frac{1}{\Delta x \Delta y}\int_{I_{i,j}} s(u_h)\mathrm{d}x\mathrm{d}y,$$

where

$$\bar{u}_{i,j} = \frac{1}{\Delta x \Delta y}\int_{I_{i,j}} u_h \mathrm{d}x\mathrm{d}y.$$

Substituting (20) and (21) into the above equation, we obtain

$$\begin{aligned}\frac{\mathrm{d}}{\mathrm{d}t}\bar{u}_{i,j} = {} & \frac{M}{\Delta x^2}\sum_{m=1}^{2} c_m \left(u^-_{i+\frac{3}{2},j} + 3u^+_{i+\frac{1}{2},j} - 5u^-_{i+\frac{1}{2},j} - 3u^+_{i-\frac{1}{2},j} + 4u^-_{i-\frac{1}{2},j}\right)\Bigg|_{y=y_m^j} \\ & + \frac{M}{\Delta y^2}\sum_{m=1}^{2} c_m \left(u^-_{i,j+\frac{3}{2}} + 3u^+_{i,j+\frac{1}{2}} - 5u^-_{i,j+\frac{1}{2}} - 3u^+_{i,j-\frac{1}{2}} + 4u^-_{i,j-\frac{1}{2}}\right)\Bigg|_{x=x_m^i} \\ & + \frac{1}{\Delta x \Delta y}\int_{I_{i,j}} s(u_h)\mathrm{d}x\mathrm{d}y. \end{aligned} \tag{22}$$

By using the temporal discretization (11) and (12), we get the following equations for updating the cell average value $\bar{u}_{i,j}$ in time:

$$\bar{u}_{i,j}^{(1)} = B_1^1\left[\bar{u}_{i,j}^n + \Delta t f\left(u_h^n\right)\right] + \Delta t B_1^1\left[\frac{1}{\Delta x \Delta y}\int_{I_{i,j}} s\left(u_h^n\right)\mathrm{d}x\mathrm{d}y + \mu \bar{u}_{i,j}^n\right], \tag{23}$$

$$\bar{u}_i^{n+1} = B_2^1 \bar{u}^n + B_2^2\left[\bar{u}_{i,j}^{(1)} + \Delta t f(u_h^{(1)})\right] + \Delta t B_2^2\left[\frac{1}{\Delta x \Delta y}\int_{I_{i,j}} s\left(u_h^{(1)}\right)\mathrm{d}x\mathrm{d}y + \mu \bar{u}_{i,j}^{(1)}\right], \tag{24}$$

where $\bar{u}_{i,j}^n$ and $\bar{u}_{i,j}^{(1)}$ are the cell averages of u_h^n and $u_h^{(1)}$ on $I_{i,j}$, respectively. For simplicity of notations, we still use f to denote the spatial discretization operator as in the one-dimensional case. But f has a different definition in the two-dimensional problem:

$$\begin{aligned} f(\omega) = {} & \frac{M}{\Delta x^2}\sum_{m=1}^{2} c_m \left(\omega^-_{i+\frac{3}{2},j} + 3\omega^+_{i+\frac{1}{2},j} - 5\omega^-_{i+\frac{1}{2},j} - 3\omega^+_{i-\frac{1}{2},j} + 4\omega^-_{i-\frac{1}{2},j}\right)\Bigg|_{y=y_m^j} \\ & + \frac{M}{\Delta y^2}\sum_{m=1}^{2} c_m \left(\omega^-_{i,j+\frac{3}{2}} + 3\omega^+_{i,j+\frac{1}{2}} - 5\omega^-_{i,j+\frac{1}{2}} - 3\omega^+_{i,j-\frac{1}{2}} + 4\omega^-_{i,j-\frac{1}{2}}\right)\Bigg|_{x=x_m^i}, \end{aligned}$$

for any function $\omega \in V_h$. We state the property of f in the following lemma.

Lemma 2 *For any function $\omega(x) \in V_h$ with $\omega \in [-1, 1]$, we have*

$$\bar{\omega}_{i,j} + \Delta t f(\omega) \in [-1, 1],$$

under the CFL condition $M\Delta t \leqslant \frac{1}{20}\min\{\Delta x^2, \Delta y^2\}$.

Proof We divide ω into two parts and use the Gaussian quadrature rule in different directions:

$$\begin{aligned}
\bar{\omega}_{i,j} &= \frac{1}{2}\bar{\omega}_{i,j} + \frac{1}{2}\bar{\omega}_{i,j} \\
&= \frac{1}{2\Delta x}\sum_{m=1}^{2} c_m \int_{x_{i-\frac{1}{2}}}^{x_{i+\frac{1}{2}}} \omega\big(x, y_m^j\big)\mathrm{d}x + \frac{1}{2\Delta y}\sum_{m=1}^{2} c_m \int_{y_{j-\frac{1}{2}}}^{y_{j+\frac{1}{2}}} \omega\big(x_m^i, y\big)\mathrm{d}y \\
&= \frac{1}{4}\sum_{m=1}^{2} c_m \left[\omega^-_{i+\frac{1}{2},j}\big(y_m^j\big) + \omega^+_{i-\frac{1}{2},j}\big(y_m^j\big)\right] + \frac{1}{4}\sum_{m=1}^{2} c_m \left[\omega^-_{i,j+\frac{1}{2}}\big(x_m^i\big) + \omega^+_{i,j-\frac{1}{2}}\big(x_m^i\big)\right].
\end{aligned}$$

Then, we obtain

$$\begin{aligned}
&\bar{\omega}_{i,j} + \Delta t f(\omega) \\
&= \sum_{m=1}^{2} c_m \left(a_1\omega^-_{i+\frac{3}{2},j} + a_2\omega^+_{i+\frac{1}{2},j} + a_3\omega^-_{i+\frac{1}{2},j} + a_4\omega^+_{i-\frac{1}{2},j} + a_5\omega^-_{i-\frac{1}{2},j}\right)\Bigg|_{y=y_m^j} \\
&\quad + \sum_{m=1}^{2} c_m \left(b_1\omega^-_{i,j+\frac{3}{2}} + b_2\omega^+_{i,j+\frac{1}{2}} + b_3\omega^-_{i,j+\frac{1}{2}} + b_4\omega^+_{i,j-\frac{1}{2}} + b_5\omega^-_{i,j-\frac{1}{2}}\right)\Bigg|_{x=y_m^i},
\end{aligned}$$

where

$$\begin{aligned}
a_1 &= \frac{M\Delta t}{\Delta x^2},\ a_2 = 3\frac{M\Delta t}{\Delta x^2},\ a_3 = \frac{1}{4} - 5\frac{M\Delta t}{\Delta x^2},\ a_4 = \frac{1}{4} - 3\frac{M\Delta t}{\Delta x^2},\ a_5 = 4\frac{M\Delta t}{\Delta x^2}, \\
b_1 &= \frac{M\Delta t}{\Delta y^2},\ b_2 = 3\frac{M\Delta t}{\Delta y^2},\ b_3 = \frac{1}{4} - 5\frac{M\Delta t}{\Delta y^2},\ b_4 = \frac{1}{4} - 3\frac{M\Delta t}{\Delta y^2},\ b_5 = 4\frac{M\Delta t}{\Delta y^2}.
\end{aligned}$$

Notice that $c_1 + c_2 = 1$ and hence it is easy to check that

$$\sum_{m=1}^{2} c_m\big(a_1 + a_2 + a_3 + a_4 + a_5\big) + \sum_{m=1}^{2} c_m\big(b_1 + b_2 + b_3 + b_4 + b_5\big) = 1.$$

If we require $M\Delta t \leqslant \frac{1}{20}\min\{\Delta x^2, \Delta y^2\}$, then all coefficients are non-negative. Hence, we have written $\bar{\omega}_{i,j} + \Delta t f(\omega)$ as a convex combination of several point values of ω. Since all point values are bounded between -1 and 1, we can obtain the conclusion of this lemma.

Finally, we get the following theorem of the maximum-principle-preserving property of the cell average values. The proof is similar to the one-dimensional case and hence we omit it. Here we denote the set of L Gauss quadrature points on $[x_{i-\frac{1}{2}}, x_{i+\frac{1}{2}}]$ as S_i^x and denote the

set of Gauss quadrature points on $[y_{j-\frac{1}{2}}, y_{j+\frac{1}{2}}]$ as S_j^y. We still choose L such that the computation for $\int_{I_{i,j}} s(u_h)\mathrm{d}x\mathrm{d}y$ is accurate enough. Moreover, we let $S_{i,j} = S_i^x \otimes S_j^y$.

Theorem 3 *Consider the ODE* (22) *of the cell average* $\bar{u}_{i,j}$, *the numerical scheme* (23) *and* (24) *is bound-preserving*: *if* $-1 \leqslant u_h^n(x,y) \leqslant 1$ *on each cell* $I_{i,j}$, $i = 1, \cdots, N_x$, $j = 1, \cdots, N_y$, *then we have* $-1 \leqslant \bar{u}_{i,j}^{(1)} \leqslant 1$ *under the conditions*

$$\mu \geqslant \max\left\{0, \max_{(x,y)\in S_{i,j}} \frac{s\left(u_h^n(x,y)\right)}{1-u_h^n(x,y)}, \max_{(x,y)\in S_{i,j}} \frac{s\left(u_h^n(x,y)\right)}{-1-u_h^n(x,y)}\right\}$$

and

$$M\Delta t \leqslant \frac{1}{20}\min\{\Delta x^2, \Delta y^2\}.$$

In addition to the above conditions, if $-1 \leqslant u_h^{(1)}(x,y) \leqslant 1$ *on each cell* $I_{i,j}$, $i = 1, \cdots, N_x$, $j = 1, \cdots, N_y$ *and*

$$\mu \geqslant \max\left\{0, \max_{(x,y)\in S_{i,j}} \frac{s\left(u_h^{(1)}(x,y)\right)}{1-u_h^{(1)}(x,y)}, \max_{(x,y)\in S_{i,j}} \frac{s\left(u_h^{(1)}(x,y)\right)}{-1-u_h^{(1)}(x,y)}\right\},$$

then we have $-1 \leqslant \bar{u}_{i,j}^{n+1} \leqslant 1$.

Now we can construct physically relevant numerical cell averages $\bar{u}_{i,j}$. However, the polynomial u_h may be out of the bounds. On each stage of the conservative modified exponential RK method, we need to replace the solution with a modified polynomial on each cell. The whole procedure is the same as the one-dimensional limiter described in Sect. 3.2. For simplicity, we only show the formulation at the time level $n+1$ for the two-dimensional case. On each cell $I_{i,j}$, after we get the polynomial $u_h^{n+1}(x,y)$ by using the temporal discretization, we replace it with a modified polynomial $\tilde{u}_h^{n+1}(x,y)$:

$$\tilde{u}_h^{n+1}(x,y) = \theta\left(u_h^{n+1}(x,y) - \bar{u}_{i,j}^{n+1}\right) + \bar{u}_{i,j}^{n+1},$$

where

$$\theta = \min\left\{1, \frac{1-\bar{u}_{i,j}^{n+1}}{M_{i,j}-\bar{u}_{i,j}^{n+1}}, \frac{\bar{u}_{i,j}^{n+1}+1}{\bar{u}_{i,j}^{n+1}-m_{i,j}}\right\}$$

and

$$M_{i,j} = \max_{(x,y)\in I_{i,j}} u_h^{n+1}(x,y), \quad m_i = \min_{(x,y)\in I_{i,j}} u_h^{n+1}(x,y).$$

Then, we can get $-1 \leqslant \tilde{u}_h^{n+1}(x,y) \leqslant 1$.

5 Numerical Examples

In this section, we take the nonlinear free energy density as

$$F(u) = \frac{1}{4\epsilon^2}(u^2 - 1)^2,$$

where ϵ represents the inter-facial width. In this case, the energy function becomes

$$E(u) = \int_\Omega \Big(\frac{1}{2}|\nabla u|^2 + \frac{1}{4\epsilon^2}(u^2 - 1)^2\Big)\mathrm{d}\mathbf{x}.$$

Also, we have

$$s(u) = -MF'(u) = \frac{M}{\epsilon^2}(u - u^3),$$

and the Allen-Cahn equation becomes

$$u_t = M\Big(\Delta u + \frac{1}{\epsilon^2}(u - u^3)\Big). \tag{25}$$

In the one-dimensional case, we have

$$u_t = M\Big(u_{xx} + \frac{1}{\epsilon^2}(u - u^3)\Big). \tag{26}$$

Although we only show the detailed formulation for the second-order scheme, we also test the third-order scheme in this section. For the spatial discretization, we follow the method in [21]. For the time integration, we adopt the method in [17], which has also been illustrated at the end of Sect. 2. We will numerically show that our method has the MPP property and test whether we can observe the energy decay. In all figures, we use "new RK" to represent the conservative modified exponential RK method and use "RK" to represent the traditional SSP RK method. Also, "without limiter" means that we do not modify the polynomials as in Sect. 3.2. But we still choose a suitable parameter μ in the conservative exponential RK method as described in Theorems 2 and 3. This parameter also helps to approach the correct solutions.

Example 1 We first test the stability and accuracy of the ODE solvers, and study the following problem:

Table 1 Accuracy test for ODE solvers with $u_0 = 0.2$ with $c = 100$

N_t	L^∞ norm	Order	L^∞ norm	Order
	Second-order new RK		Third-order new RK	
2	2.20E−09	–	2.03E−11	–
4	5.53E−10	1.99	2.54E−12	3.00
8	1.39E−10	1.99	3.17E−13	3.00
16	3.47E−11	2.00	3.95E−14	3.00
32	8.69E−12	2.00	4.88E−15	3.02

$$u'(t) = -cu^7, \quad u(0) = u_0,$$

where c is a parameter that we can adjust. The problem becomes stiff as c increases. The exact solution is

$$u(t) = u_0\left(6ctu_0^6 + 1\right)^{-1/6}.$$

We take the final time to be $t = 0.5$ and denote the total number of time steps as N_t.

We first take $u_0 = 0.2$ with $c = 100$. We choose $c = 100$ because in most of the previous works for Allen-Cahn equations, the value of $1/\epsilon \approx 100$. Numerical results for the second-order and third-order new RK method are listed in Table 1. The initial condition is well-prepared, and we can observe the optimal convergence rates.

Next, we take $u_0 = 1$, the results are given in Table 2. For this problem, the initial condition is not well-prepared, and we can observe the optimal convergence rate if the problem is not stiff, e.g., $c = 1$. If the problem is stiff, e.g., $c = 100$, the method may not converge at the expected rate, but our scheme is able to deal with large time steps and we can observe the convergence of the solutions.

Example 2 We consider the one-dimensional Allen-Cahn equation (26) with periodic boundary conditions. We take $M = 1$ and adopt $N = 100$ cells. The computational domain is $[0, 2\pi]$ and the initial condition is taken as

$$u(x, 0) = \sin(x).$$

We first test the second-order schemes. We adopt the new RK method and compare the results with and without the MPP limiter in Fig. 1. Different values of ϵ are tested. The time step size $\Delta t = c\Delta x^2/M$ with $c = 0.1$ is used in all cases. We can see that the energy decays as the time increases. The maximum principle is preserved after we add the MPP limiter.

Next, we take $\mu = 0$, then the new RK method becomes the regular second-order RK method. In this case, the code will blow up with the same choice of Δt as in the new RK

Table 2 Accuracy test for ODE solvers with $u_0 = 1$

N_t	c=1		c=100	
	L^∞ norm	Order	L^∞ norm	Order
	Second-order new RK			
20	1.84E−05	–	9.40E−02	–
40	5.08E−06	1.86	1.00E−02	3.23
80	1.31E−06	1.95	7.63E−04	3.71
160	3.36E−07	1.97	6.35E−05	3.59
320	8.50E−08	1.98	2.19E−06	4.86
	Third-order new RK			
20	2.04E−06	–	2.67E−02	–
40	2.51E−07	3.02	1.27E−03	4.39
80	3.08E−08	3.03	1.00E−04	3.67
160	3.85E−09	3.00	2.00E−05	2.32
320	4.82E−10	3.00	3.32E−06	2.59

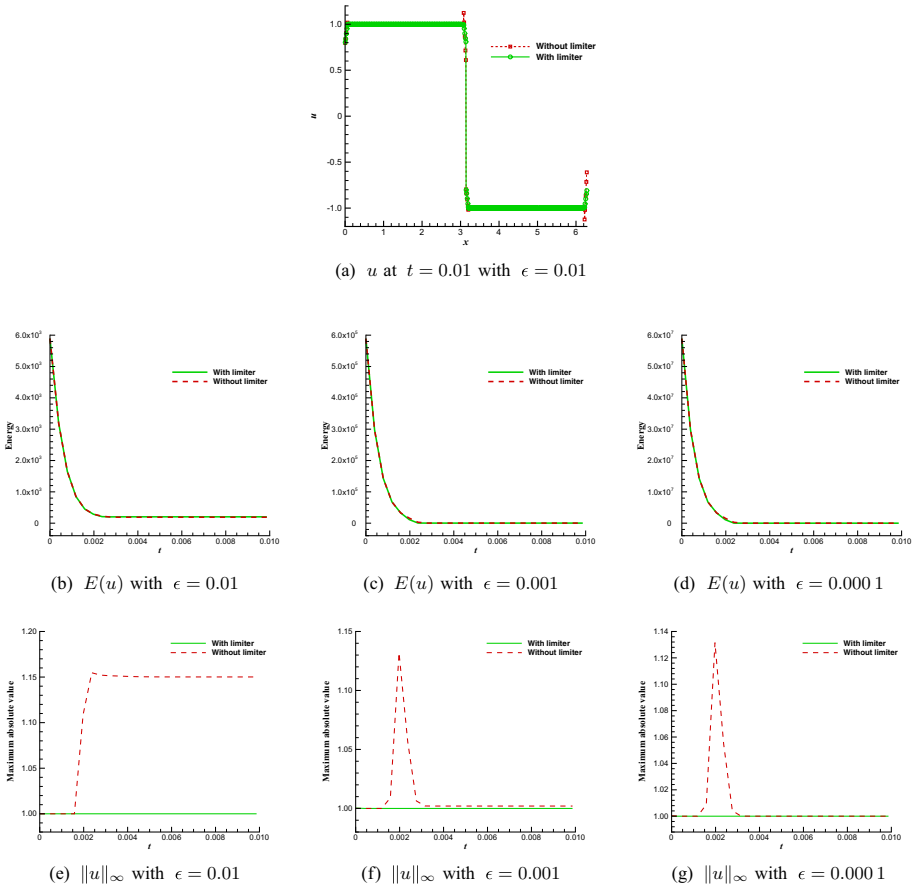

(a) u at $t = 0.01$ with $\epsilon = 0.01$

(b) $E(u)$ with $\epsilon = 0.01$ (c) $E(u)$ with $\epsilon = 0.001$ (d) $E(u)$ with $\epsilon = 0.000\,1$

(e) $\|u\|_\infty$ with $\epsilon = 0.01$ (f) $\|u\|_\infty$ with $\epsilon = 0.001$ (g) $\|u\|_\infty$ with $\epsilon = 0.000\,1$

Fig. 1 Example 2 with different ϵ. Second-order method with new RK. Comparison of results with and without the MPP limiter. $\Delta t = c\Delta x^2/M$ with $c = 0.1$

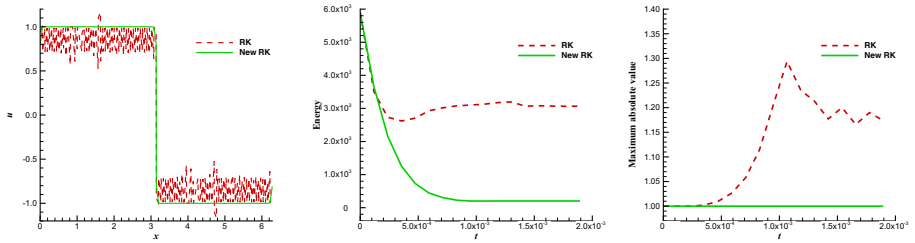

(a) u at $t = 0.02$ **(b)** $E(u)$ **(c)** $\|u\|_\infty$

Fig. 2 Example 2 with $\epsilon = 0.01$. Second-order schemes with MPP limiters. Comparison between RK and new RK methods. $\Delta t = c\Delta x^2/M$ with $c = 0.03$

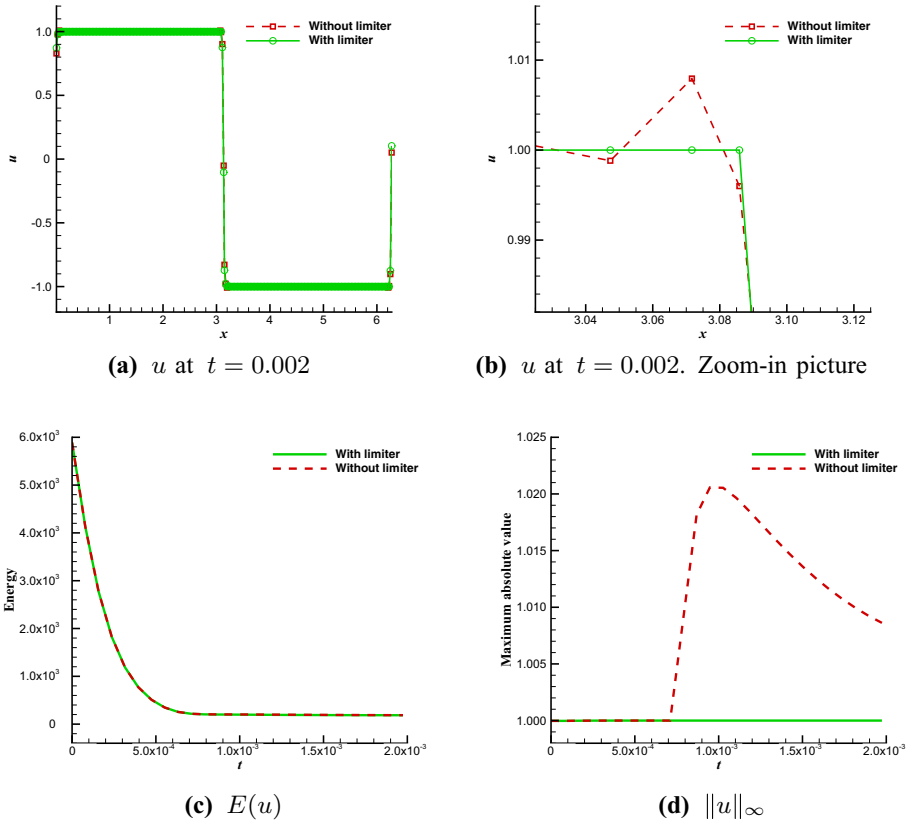

(a) u at $t = 0.002$ **(b)** u at $t = 0.002$. Zoom-in picture

(c) $E(u)$ **(d)** $\|u\|_\infty$

Fig. 3 Example 2 with $\epsilon = 0.01$. Third-order method with new RK. Comparison of results with and without the MPP limiter. $\Delta t = c\Delta x^2/M$ with $c = 0.02$

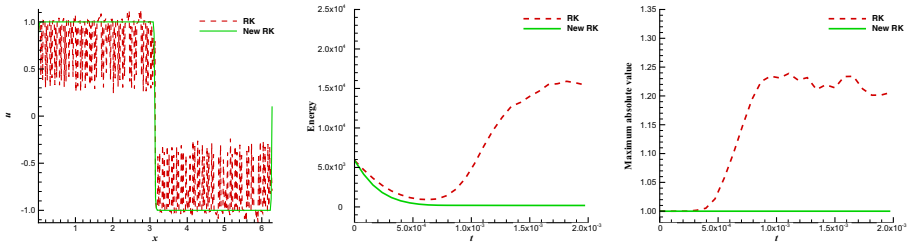

(a) u at $t = 0.02$ **(b)** $E(u)$ **(c)** $\|u\|_\infty$

Fig. 4 Example 2 with $\epsilon = 0.01$. Third-order schemes with MPP limiters. Comparison between RK and new RK methods. $\Delta t = c\Delta x^2/M$ with $c = 0.02$

method. For comparison, we take $\epsilon = 0.01$ and $\Delta t = c\Delta x^2/M$ with $c = 0.03$. The results of different methods are shown in Fig. 2. We can see that the traditional RK method will lead to wrong solutions. To obtain correct solutions, $c = 0.01$ is needed. For $\epsilon = 0.001$, $c = 10^{-4}$ is needed in traditional RK method. If we take $\epsilon = 0.000\,1$, then $c = 10^{-6}$ is needed.

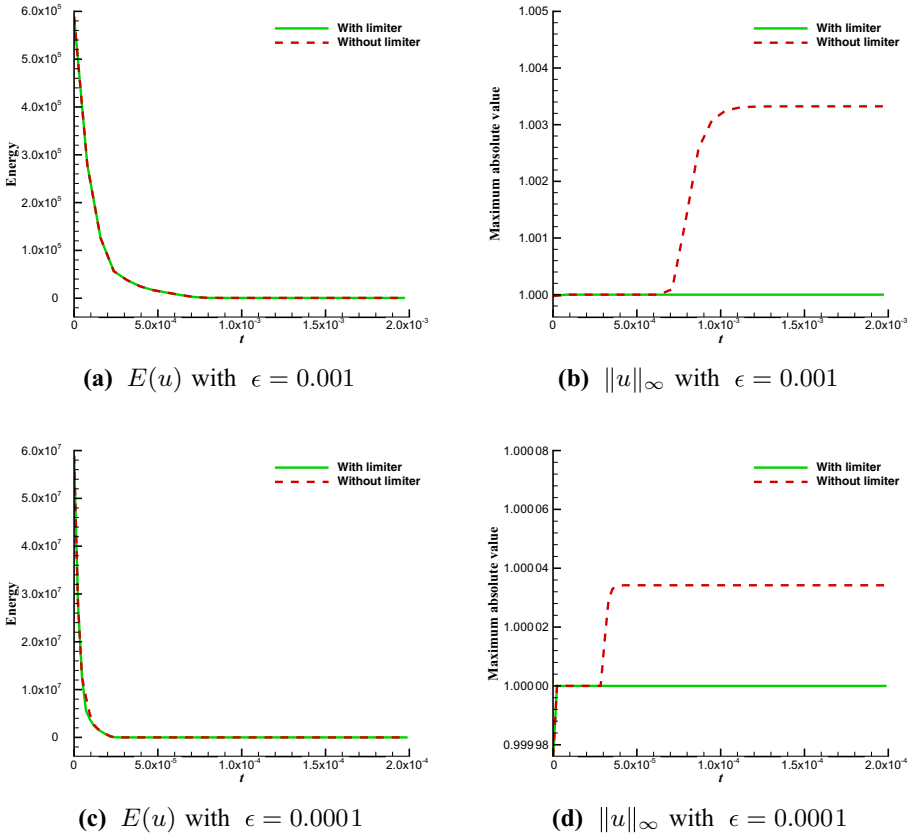

(a) $E(u)$ with $\epsilon = 0.001$ **(b)** $\|u\|_\infty$ with $\epsilon = 0.001$

(c) $E(u)$ with $\epsilon = 0.0001$ **(d)** $\|u\|_\infty$ with $\epsilon = 0.0001$

Fig. 5 Example 2 with different ϵ. Third-order scheme with new RK. $\Delta t = c\Delta x^2/M$. We take with $c = 0.02$ for $\epsilon = 0.001$, and take $c = 6 \times 10^{-4}$ for $\epsilon = 0.000\,1$

We move on to test the third-order schemes. Firstly, we take $\epsilon = 0.01$ and adopt the new RK method in time. The time step size $\Delta t = c\Delta x^2/M$ with $c = 0.02$ is used. The numerical methods with and without the MPP limiter are shown in Fig. 3. We can see that the energy decays as the time increases. The maximum principle is preserved after we add the MPP limiter. Next, we still take $\epsilon = 0.01$ and compare our new RK method with the traditional RK method in Fig. 4. The same time step size with $c = 0.02$ is used. We can see that the traditional RK method leads to wrong solutions. To obtain correct solutions with the traditional RK method, we need to take $c = 6 \times 10^{-3}$. Finally, we test smaller values of ϵ. The numerical results of our new RK method are shown in Fig. 5. Here we take with $c = 0.02$ for $\epsilon = 0.001$, and take $c = 6 \times 10^{-4}$ for $\epsilon = 0.000\,1$. Again, we can see that the energy decays and the MPP property is preserved. For $\epsilon = 0.001$, if we still use $c = 0.02$ in the traditional RK method, the code will blow up, and $c = 10^{-4}$ is needed to obtain correct solutions. For $\epsilon = 0.000\,1$, $c = 10^{-6}$ is needed in the traditional RK method.

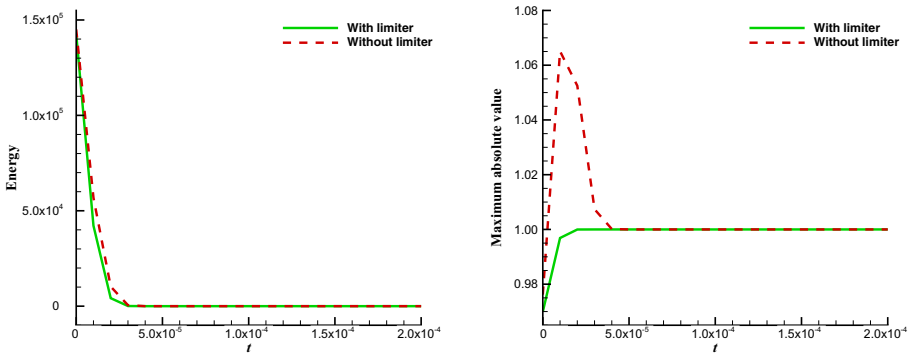

(a) $E(u)$ **(b)** $\|u\|_\infty$

Fig. 6 Example 3

Example 3 We consider the one-dimensional Allen-Cahn equation (26) with homogeneous Neumann boundary conditions. We take $M = 1$ and $\epsilon = 0.001$. The computation domain is [0, 1] and the initial condition is chosen as

$$u(x, 0) = 0.9 \times \text{rand}(\cdot) + 0.05,$$

where "rand(·)" represents a random number on each point in [0, 1].

From now on, we only test the second-order schemes for simplicity. We take $N = 100$ cells and compare the results with and without the MPP limiter in Fig. 6. The time step size $\Delta t = c\Delta x^2/M$ with $c = 0.1$ is used. We can observe that the energy decays as the time increases. The maximum principle is preserved after we add the MPP limiter. Again, if we do not add the limiter and further take $\mu = 0$, the code will blow up with the same choice of Δt.

Example 4 We consider the two-dimensional Allen-Cahn equation (25) with periodic boundary conditions. We take $M = 0.01$ and $\epsilon = 0.08$. The computational domain is $[0, 1] \times [0, 1]$. The initial condition is taken as

$$u(x, y, 0) = \cos(\pi x)\cos(\pi y).$$

Table 3 Two-dimensional accuracy test

N	Without limiter				With MPP limiter			
	L^2 norm	Order	L^∞ norm	Order	L^2 norm	Order	L^∞ norm	Order
20	2.15E−02	–	1.02E−01	–	2.08E−02	–	9.10E−02	–
40	4.79E−03	2.17	2.95E−02	1.79	4.78E−03	2.12	2.52E−02	1.85
80	1.16E−03	2.04	7.39E−03	2.00	1.18E−03	2.02	6.41E−03	1.97
160	2.87E−04	2.02	1.86E−03	1.99	2.93E−04	2.01	1.60E−03	2.00

We divide the computational domain into $N \times N$ cells, i.e., $N_x = N_y = N$. The time step size $\Delta t = 0.02\Delta x^2/M$ is used. Table 3 shows the numerical errors at the time $T = 0.5$. We can observe the second-order convergence rate. Also, the MPP limiter does not harm the original high order of accuracy.

Example 5 We solve a benchmark problem for the two-dimensional Allen-Cahn equation (25). Consider a two-dimensional domain $(-128, 128)^2$ with a circle of radius $R_0 = 100$. In other words, the initial condition is given by

$$u(x, y, 0) = \begin{cases} 1, & \text{if } x^2 + y^2 < 100^2, \\ -1, & \text{otherwise.} \end{cases}$$

The boundary condition is taken as the periodic boundary condition. By mapping the domain to $\Omega = (-1, 1)^2$, the parameters in the two-dimensional Allen-Cahn equation are given by $M = 6.103\,51 \times 10^{-5}$ and $\epsilon = 0.007\,8$. In the sharp interface limit ($\epsilon \to 0$, which is suitable because the chosen ϵ is small), the radius at the time t should be

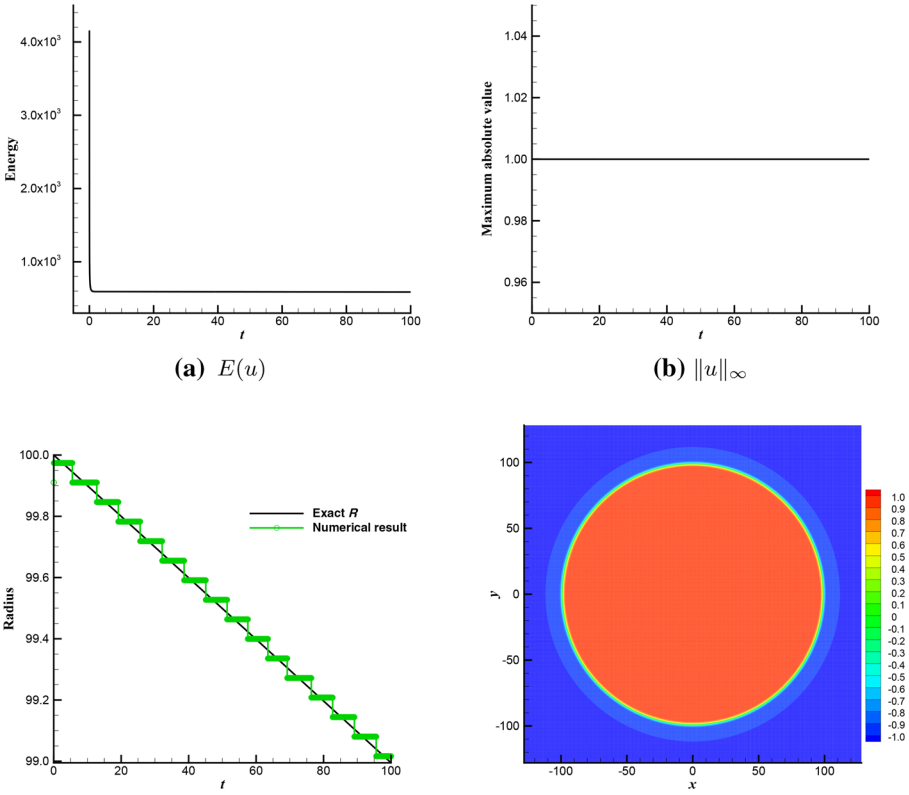

(a) $E(u)$ **(b)** $\|u\|_\infty$

(c) R **(d)** u at $t = 100$

Fig. 7 Example 5

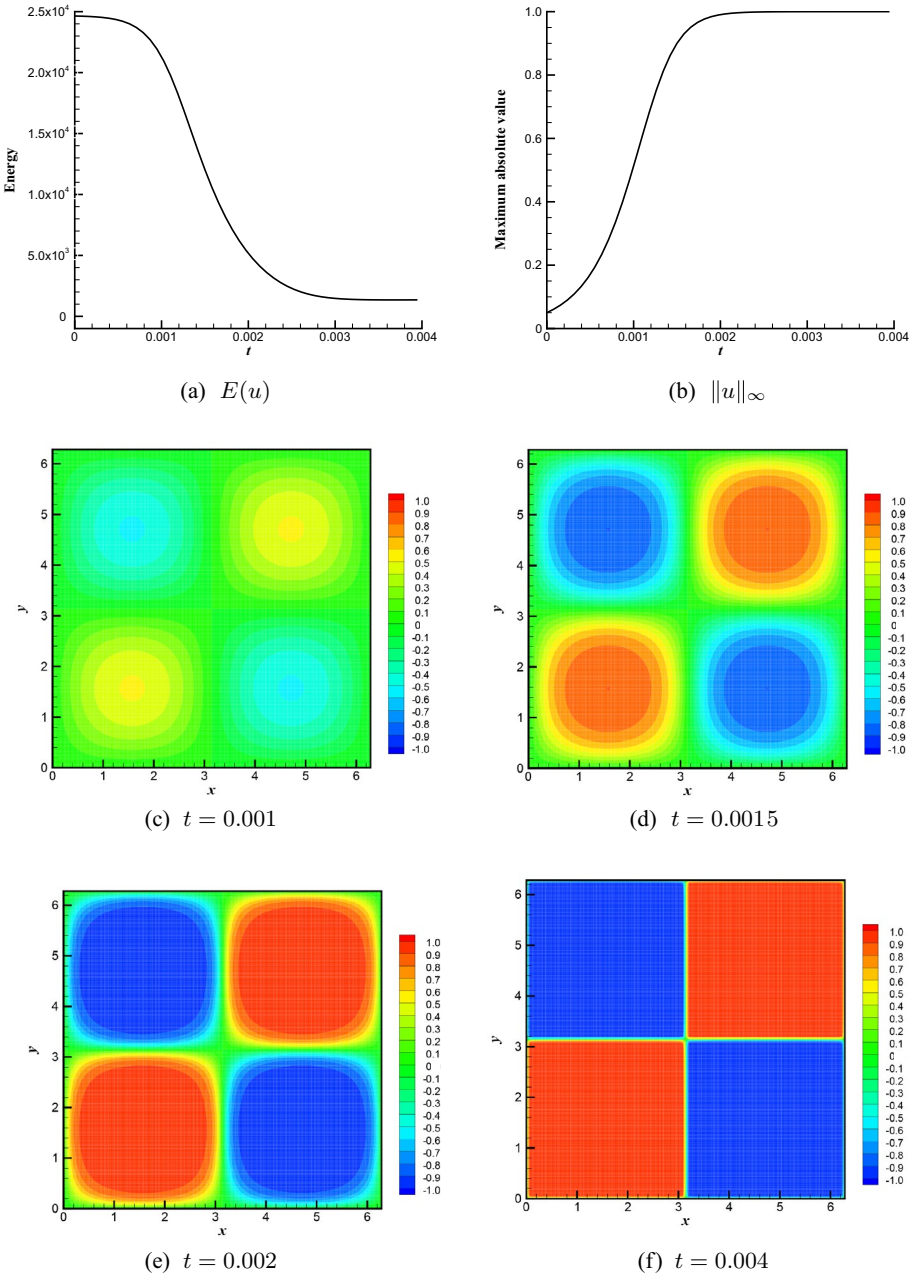

(a) $E(u)$ (b) $\|u\|_\infty$

(c) $t = 0.001$ (d) $t = 0.0015$

(e) $t = 0.002$ (f) $t = 0.004$

Fig. 8 Example 6

$$R = \sqrt{R_0^2 - 2t}.$$

We take $N_x = N_y = 401$. The time step size is $\Delta t = 0.02\Delta x^2/M$. We add the MPP limiter. Numerical results are shown in Fig. 7. We can see that the energy decays and the maximum principle is preserved. Also, we compare the real radius R with the numerical one. We can see that our method can capture the correct radius.

Example 6 We consider the two-dimensional Allen-Cahn equation (25) with periodic boundary conditions. We take $M = 1$ and $\epsilon = 0.02$. The computational domain is $[0, 2\pi]^2$. The initial condition is taken as $u(x, y, 0) = 0.05 \sin(x) \sin(y)$.

We adopt $N_x = N_y = 100$. The time step size is $\Delta t = 0.02\Delta x^2/M$. We add the MPP limiter. Numerical results are shown in Fig. 8. We can see that the energy decays as the time increases. The maximum principle is preserved. Also, we can observe the phase separation and coarsening process.

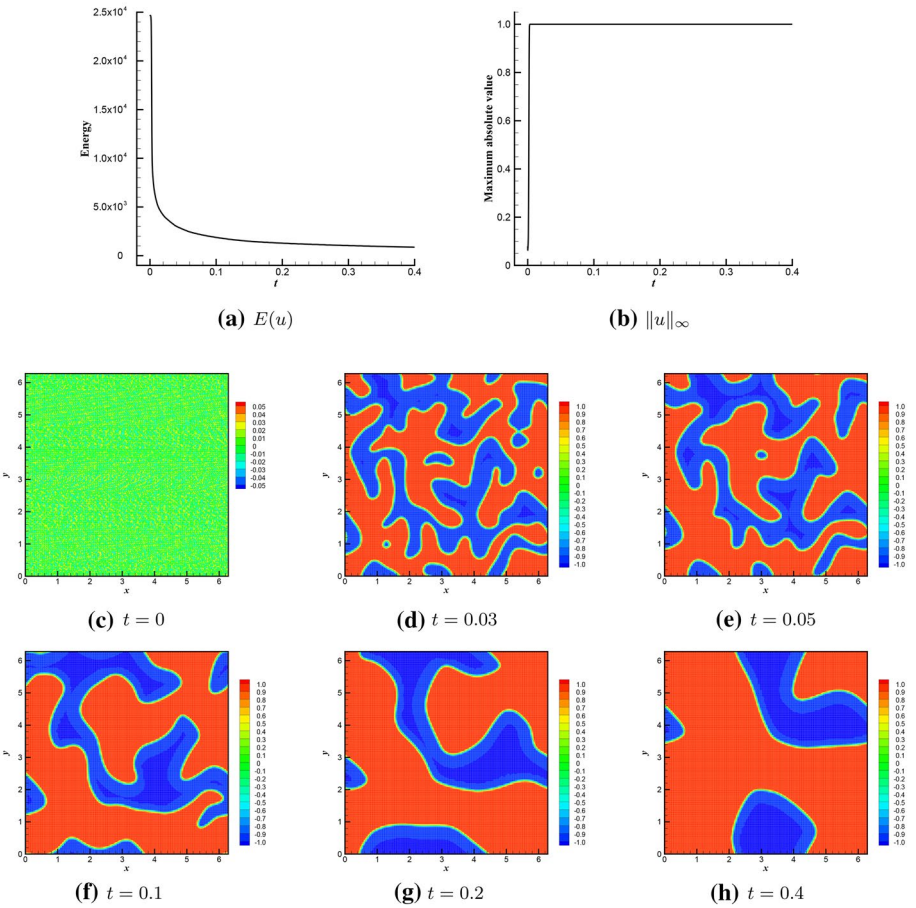

(a) $E(u)$ **(b)** $\|u\|_\infty$

(c) $t = 0$ **(d)** $t = 0.03$ **(e)** $t = 0.05$

(f) $t = 0.1$ **(g)** $t = 0.2$ **(h)** $t = 0.4$

Fig. 9 Example 7

Example 7 We consider the two-dimensional Allen-Cahn equation (25) with periodic boundary conditions. We take $M = 1$ and $\epsilon = 0.02$. The computational domain is $[0, 2\pi]^2$. The initial condition is a random function with values in $[-0.05, 0.05]$.

We adopt $N_x = N_y = 100$. The time step size is $\Delta t = 0.02\Delta x^2/M$. The MPP limiter is added. The plots of energy and the maximum absolute value are shown in Fig. 9. We can see that the energy decays as the time increases. The maximum principle is preserved. The plots of u at different times are also shown in Fig. 9. We can observe the phase separation and coarsening process.

6 Conclusion

In this paper, we study the classical Allen-Cahn equations. We apply the LDG method due to its flexibility on the *h-p* adaptivity and complex geometry. Moreover, since the source given in the equation may be stiff, we use the conservative modified exponential RK methods and thus can use relatively large time step sizes. Thanks to the conservative time integration, we can design the MPP technique for the scheme. Moreover, the physical bounds of the unknown function will not decay. Numerical experiments are also given to demonstrate the good performance of the MPP LDG scheme.

Since the MPP LDG methods require slope limiters, the energy stability may not be easy to obtain. In this paper, we only discuss the MPP technique and use numerical experiments to demonstrate the energy decay property. The proof for the energy decay will be investigated in the future.

Funding Jie Du is supported by the National Natural Science Foundation of China under Grant Number NSFC 11801302 and Tsinghua University Initiative Scientific Research Program. Eric Chung is supported by Hong Kong RGC General Research Fund (Projects 14304217 and 14302018). The third author is supported by the NSF grant DMS-1818467.

Compliance with Ethical Standards

Conflict of interest On behalf of all authors, the corresponding author states that there is no conflict of interest.

References

1. Arnold, D.: An interior penalty finite element method with discontinuous elements. SIAM J. Numer. Anal. **19**, 742–760 (1982)
2. Bassi, F., Rebay, S.: A high-order accurate discontinuous finite element method for the numerical solution of the compressible Navier-Stokes equations. J. Comput. Phys. **131**, 267–279 (1997)
3. Cahn, J.W., Hilliard, J.E.: Free energy of a nonuniform system. I. Interfacial free energy. J. Chem. Phys. **28**, 258–267 (1958)
4. Cahn, J.W., Hilliard, J.E.: Free energy of a nonuniform system. III. Nucleation in a two-component incompressible fluid. J. Chem. Phys. **31**, 688–699 (1959)
5. Chen, Z., Huang, H., Yan, J.: Third order maximum-principle-satisfying direct discontinuous Galerkin method for time dependent convection diffusion equations on unstructured triangular meshes. J. Comput. Phys. **308**, 198–217 (2016)
6. Cheng, Y., Shu, C.-W.: A discontinuous Galerkin finite element method for time dependent partial differential equations with higher order derivatives. Math. Comput. **77**, 699–730 (2008)

7. Chuenjarern, N., Xu, Z., Yang, Y.: High-order bound-preserving discontinuous Galerkin methods for compressible miscible displacements in porous media on triangular meshes. J. Comput. Phys. **378**, 110–128 (2019)
8. Chung, E., Lee, C.S.: A staggered discontinuous Galerkin method for convection-diffusion equations. J. Numer. Math. **20**, 1–31 (2012)
9. Cockburn, B., Hou, S., Shu, C.-W.: The Runge-Kutta local projection discontinuous Galerkin finite element method for conservation laws. IV: the multidimensional case. Math. Comput. **54**, 545–581 (1990)
10. Cockburn, B., Lin, S.Y., Shu, C.-W.: TVB Runge-Kutta local projection discontinuous Galerkin finite element method for conservation laws. III: one-dimensional systems. J. Comput. Phys. **84**, 90–113 (1989)
11. Cockburn, B., Shu, C.-W.: TVB Runge-Kutta local projection discontinuous Galerkin finite element method for conservation laws. II: general framework. Math. Comput. **52**, 411–435 (1989)
12. Cockburn, B., Shu, C.-W.: The Runge-Kutta discontinuous Galerkin method for conservation laws. V: Multidimensional systems. J. Comput. Phys. **141**, 199–224 (1998)
13. Cockburn, B., Shu, C.-W.: The local discontinuous Galerkin method for time-dependent convection-diffusion systems. SIAM J. Numer. Anal. **35**, 2440–2463 (1998)
14. Du, J., Chung, E.: An adaptive staggered discontinuous Galerkin method for the steady state convection-diffusion equation. J. Sci. Comput. **77**, 1490–1518 (2018)
15. Du, J., Wang, C., Qian, C., Yang, Y.: High-order bound-preserving discontinuous Galerkin methods for stiff multispecies detonation. SIAM J. Sci. Comput. **41**, B250–B273 (2019)
16. Du, J., Yang, Y.: Maximum-principle-preserving third-order local discontinuous Galerkin methods on overlapping meshes. J. Comput. Phys. **377**, 117–141 (2019)
17. Du, J., Yang, Y.: Third-order conservative sign-preserving and steady-state-preserving time integrations and applications in stiff multispecies and multireaction detonations. J. Comput. Phys. **395**, 489–510 (2019)
18. Du, J., Yang, Y., Chung, E.: Stability analysis and error estimates of local discontinuous Galerkin method for convection-diffusion equations on overlapping meshes. BIT Numer. Math. **59**, 853–876 (2019)
19. Du, Q., Ju, L., Li, X., Qiao, Z.: Maximum principle preserving exponential time differencing schemes for the nonlocal Allen-Cahn equation. SIAM J. Numer. Anal. **57**, 875–898 (2018)
20. Gottlieb, S., Shu, C.-W., Tadmor, E.: Strong stability-preserving high-order time discretization method. SIAM Rev. **43**, 89–112 (2001)
21. Guo, L., Yang, Y.: Positivity-preserving high-order local discontinuous Galerkin method for parabolic equations with blow-up solutions. J. Comput. Phys. **289**, 181–195 (2015)
22. Guo, H., Yang, Y.: Bound-preserving discontinuous Galerkin method for compressible miscible displacement problem in porous media. SIAM J. Sci. Comput. **39**, A1969–A1990 (2017)
23. Hou, T.L., Tang, T., Yang, J.: Numerical analysis of fully discretized Crank-Nicolson scheme for fractional-in-space Allen-Cahn equations. J. Sci. Comput. **72**, 1214–1231 (2017)
24. Huang, J., Shu, C.-W.: Bound-preserving modified exponential Runge-Kutta discontinuous Galerkin methods for scalar hyperbolic equations with stiff source terms. J. Comput. Phys. **361**, 111–135 (2018)
25. Li, X., Shu, C.-W., Yang, Y.: Local discontinuous Galerkin method for the Keller-Segel chemotaxis model. J. Sci. Comput. **73**, 943–967 (2017)
26. Liu, H., Yan, J.: The direct discontinuous Galerkin methods for diffusion problems. SIAM J. Numer. Anal. **47**, 675–698 (2009)
27. Liu, Y., Shu, C.-W., Tadmor, E., Zhang, M.: Central local discontinuous Galerkin method on overlapping cells for diffusion equations. ESAIM Math. Model. Numer. Anal. **45**, 1009–1032 (2011)
28. Reed, W.H., Hill, T.R.: Triangular mesh method for the neutron transport equation. Los Alamos Scientific Laboratory Report LA-UR-73-479, Los Alamos (1973)
29. Riviere, B., Wheeler, M.F., Girault, V.: Improved energy estimates for interior penalty, constrained and discontinuous Galerkin methods for elliptic problems. Part I. Comput. Geosci. **8**, 337–360 (1999)
30. Shen, J., Tang, T., Yang, J.: On the maximum principle preserving schemes for the generalized Allen-Cahn equation. Commun. Math. Sci. **14**, 1517–1534 (2016)
31. Shen, J., Xu, J., Yang, J.: A new class of efficient and robust energy stable schemes for gradient flows. SIAM Rev. **61**, 474–506 (2019)
32. Shen, J., Xu, J., Yang, J.: The scalar auxiliary variable (SAV) approach for gradient flows. J. Comput. Phys. **353**, 407–416 (2018)
33. Shen, J., Yang, X.: Numerical approximations of Allen-Cahn and Cahn-Hilliard equations. Discrete Contin. Dyn. Syst. **28**, 1669–1691 (2010)

34. Srinivasan, S., Poggie, J., Zhang, X.: A positivity-preserving high order discontinuous Galerkin scheme for convection-diffusion equations. J. Comput. Phys. **366**, 120–143 (2018)
35. Tang, T., Yang, J.: Implicit-explicit scheme for the Allen-Cahn equation preserves the maximum principle. J. Comput. Math. **34**, 471–481 (2016)
36. Wang, C., Wise, S., Lowengrub, J.: An energy-stable and convergent finite-difference scheme for the phase field crystal equation. SIAM J. Numer. Anal. **47**, 2269–2288 (2009)
37. Wheeler, M.: An elliptic collocation finite element method with interior penalties. SIAM J. Numer. Anal. **15**, 152–161 (1978)
38. Xiong, T., Qiu, J.-M., Xu, Z.: High order maximum-principle-preserving discontinuous Galerkin method for convection-diffusion equations. SIAM J. Sci. Comput. **37**, A583–A608 (2015)
39. Xu, C., Tang, T.: Stability analysis of large time-stepping methods for epitaxial growth models. SIAM J. Numer. Anal. **44**, 1759–1779 (2006)
40. Xu, Z., Yang, Y., Guo, H.: High-order bound-preserving discontinuous Galerkin methods for wormhole propagation on triangular meshes. J. Comput. Phys. **390**, 323–341 (2019)
41. Yang, X.: Linear, first and second-order, unconditionally energy stable numerical schemes for the phase field model of homopolymer blends. J. Comput. Phys. **327**, 294–316 (2016)
42. Yang, X., Han, D.: Linearly first- and second-order, unconditionally energy stable schemes for the phase field crystal model. J. Comput. Phys. **330**, 1116–1134 (2017)
43. Zhang, X., Shu, C.-W.: On maximum-principle-satisfying high order schemes for scalar conservation laws. J. Comput. Phys. **229**, 3091–3120 (2010)
44. Zhang, Y., Zhang, X., Shu, C.-W.: Maximum-principle-satisfying second order discontinuous Galerkin schemes for convection-diffusion equations on triangular meshes. J. Comput. Phys. **234**, 295–316 (2013)